Energy & Environmental Science

Accepted Manuscript

ROYAL SOCIETY OF CHEMISTRY

www.rsc.org/ees

Cooperative kinetics of depolarization in $CH_3NH_3PbI_3$ perovskite solar cells

Luca Bertoluzzi[1], Rafael S. Sanchez[1], Linfeng Liu[2], Jin-Wook Lee[3], Elena Mas-Marza,[1] Hongwei Han[2], Nam-Gyu Park[3], Ivan Mora-Sero[1], Juan Bisquert[1,4]*

[1]Photovoltaics and Optoelectronic Devices Group, Departament de Física, Universitat Jaume I, 12071 Castelló, Spain

[2]Michael Grätzel Center for Mesoscopic Solar Cells, Wuhan National Laboratory for Optoelectronics, School of Optical and Electronic Information, Huazhong University of Science and Technology, Wuhan 430074, Hubei, People's Republic of China.

[3]School of Chemical Engineering and Department of Energy Science, Sungkyunkwan University, Suwon 440-746, South Korea

[4]Department of Chemistry, Faculty of Science, King Abdulaziz University, Jeddah, Saudi Arabia

Corresponding author: bisquert@uji.es

Abstract

Despite the large photovoltaic performance recently achieved, many aspects of the working principles of hybrid organic-inorganic perovskite solar cells remain to be unveiled. We analyze the experimental features observed in the decay of photovoltage and provide an interpretation of the different depolarization regimes at distinct time scales. We introduce an instantaneous relaxation time that shows the type of relaxation for each separate mechanism. The decay of photovoltage is characterized by electronic events at short ms timescale followed by a power law relaxation in the 10-100 s time window. The latter process is associated with the slow polarization kinetics of $CH_3NH_3PbI_3$ perovskite and it points out to cooperative kinetics of polarization and depolarization of ferroelectric domains. These findings provide an important tool for interpretation of kinetic features in the perovskite ferroic solar cells.

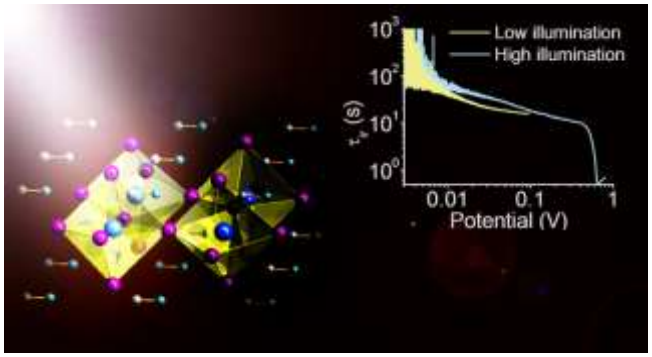

Power law voltage decay in perovskite solar cells shows cooperative relaxation phenomena

Broader context

This work describes the transient phenomena that occurs in hybrid $CH_3NH_3PbI_3$ perovskite by measurement of the decay of a photovoltage. This analysis is important in order to understand the coupled electronic-structural phenomena that take place in the operation of the perovskite solar cell, including the possible structural and electrical transformations. The results of our analysis show a separation of the decay stages into two distinct phenomena. Firstly, there are rapid electronic transients in the ms time scale, which are ordinary response times in all kind of solar cells. The novel behaviour is a slow decay in the 100 s timescale that shows a power law decay that is common in cooperative relaxations as those occurring in polymers and glassy materials. These effects evidence that the perovskite undergoes slow changes in adaptation to external perturbations, very likely associated to the ferroic behaviour of these perovskites. These finding are important for a general analysis of the perovskite and other ferroic solar cells, as these cells have an important degree of freedom, that is the internal state of polarization, that was absent in previous photovoltaic technologies.

Hybrid organic-inorganic ABX_3 perovskite solar cells (PSCs), where A is an organic cation, B is a metal and X halide atoms, are currently the best candidates for the third generation devices performing the light to electric power conversion. In particular $CH_3NH_3PbI_3$ perovskite has provided very large solar energy conversion efficiency of certified efficiencies of 20.1%.[1,2] Despite the growing amount of publications reporting enhancement of the conversion efficiency, many aspects of the working principles of such solar cells remain still uncertain.

Time transient experiments that probe the decay of electrical or optical properties are widely used to obtain the properties of charge generation, recombination and the fundamental mechanisms of voltage and current generation in hybrid organic-inorganic solar cells.[3] These transient decays such as Transient Absorption Spectroscopy (TAS), Transient Photovoltage Decays (TPD) and open-circuit voltage decay (OCVD),[4] have been normally interpreted in terms of electronic processes in a rigid organic-inorganic lattice framework. However, recent reports have revealed a new component in the dynamic response of PSCs: the dielectric relaxation (or polarization) that affects electronic processes in the absorber The origin of this process is associated to the distortable structure of the hybrid ABX_3 which causes a giant dielectric constant and the corresponding ferroelectric behaviour[5, 6] It has been shown that the dielectric-ferroelectric effects are strongly affected by voltage or light perturbation, being responsible for slow dynamic processes as manifested in voltage[7] and photocurrent decay.[8] Moreover, the application of a voltage or charge generation process to a PSC generates two distinct kinds of net charges. The first one is composed of electrons and holes, of density n and p, distributed in the volume of the absorber. The second type is related to the polarization, P, defined as the electric dipole per unit volume. This polarization, provokes bound ionic charge at the outer faces of the perovskite sample.

In order to obtain a suitable description of time transient behavior of PSC it is necessary to consider the decay of both out of equilibrium minority carrier, n and the polarization, P. In this Communication we present the experimental decays of both OCVD and TPD, describing them in terms of the combined ionic-electronic depolarization characteristics.

The photovoltage V in all solar cells is given by the difference of the Fermi level of electrons at the electron selective contact, to the Fermi level of holes at the hole selective contact.[9, 10] This separation is caused by the modification of a minority carrier Fermi level by photogenerated carriers, as $n = n_0 \exp(qV/k_BT)$, where q is the elementary charge and k_BT the thermal energy, or by the change of both electron and hole Fermi levels if the material is intrinsic. Recombination regulates the voltage decay according to a kinetic model of the type [11-13]

$$\frac{dn}{dt} = -\frac{n}{\tau_{rec}} \qquad (1)$$

Here τ_{rec} is the recombination lifetime of the minority carrier that is

$$\tau_{rec} = R_{rec} C_{\mu} \quad (2)$$

where C_{μ} is the chemical capacitance[14] and R_{rec} is the recombination resistance.[13]

In 2003 we introduced[4] the OCVD method that measures the decay of open-circuit voltage towards dark equilibrium value ($V = 0$). It was shown that the recombination time is well described by the expression

$$\tau_{rec} = -\frac{k_B T}{q}\left(\frac{dV}{dt}\right)^{-1} \quad (3)$$

It should also be remarked that the time constant measured by the reciprocal voltage derivative is not generally related to recombination.[13] In the presence of a contact capacitance, C_{co}, such as the depletion layer at the semiconductor-metal interface, the time constant $\tau_s = R_{rec} C_{co}$ does not contain information on carrier recombination lifetime. We have recently shown that depletion layer exists at the TiO_2/perovskite contact,[15] hence the interfacial capacitance must be included in a general analysis of perovskite solar cells.

A ferroelectric material is able to obtain a permanent polarization in the absence of an applied electric field. Even if the permanent polarization is not induced, the polar material creates a polarization vector P in response, and opposite to, an applied field E. There are different factors influencing the orientation of dipoles in a polar material: minimization of electrostatic energy and mechanical stress, the orientation imposed by preferred crystallographic directions, and the structural boundary conditions. The combination of these factors usually causes that the polarization is not homogenous but rather is split into distinct regions with uniformly oriented polarization called ferroelectric domains. These uniform regions are separated by domain walls that contain net ionic charge. The domain structure reduces the overall polarization and decreases the importance of depolarizing field associated to surface charge of the ferroelectric film.

The polarization P in hybrid perovskites may arise from three major mechanisms: the ionic off-centering, the atomic BX_6 cage rotations, and the organic cation dipolar orientation. The rotation of the PbI_6 octahedron is considered to be the order parameter of the cubic-tetragonal transition that occurs at 327 K.[16] The rotation of dipolar $CH_3NH_3^+$ is suggested as a source of polarization, however, the flip of the dipole is extremely fast, on picosecond scale,[17] and it should not be the main candidate for ultraslow relaxation phenomena observed in $CH_3NH_3PbI_3$. However, the size of organic cation determines properties of the primitive cell of the perovskite and consequently influencing the other polarization mechanisms. A macroscopic manifestation of polarization in the $CH_3NH_3PbI_3$ layer is the dielectric relaxation capacitance, C_{dr}, which in the limit of infinitely small frequency should be $C_{dr} = dP/dV$. A large dielectric constant has been determined[5] by measurement of C_{dr} and it has been shown to be greatly affected by illumination. The ferroelectric domains have been observed[6] and they are found to influence different cell response features. One important observation is the change of current voltage curve according to past voltage treatment.[7,

18

In this paper we consider the decay of the photovoltage that can be measured in two different types of perturbation. The TPD method is usually associated to a small perturbation of a steady state. On the other hand in the OCVD method the full photovoltage decays to the state of dark equilibrium. The photovoltage, caused by separation of Fermi levels as mentioned above, produces a corresponding modification of the internal difference of electrostatic potential from one contact to the other. The recent spatially resolved measurement of the vacuum level reveal that internal bandbending is located mainly in $CH_3NH_3PbI_3$ layer and to a much less extent in the mesoscopic $TiO_2/CH_3NH_3PbI_3$ layer.[19] The depletion layer has a great significance in ferroelectric devices, as the largest electrical field is situated in the space charge layer. Therefore the polarization by external bias can affect substantially the depletion layer more than the quasi-neutral regions.[15, 19] Under illumination the vacuum level changes by about 1 V over a thickness of order 1 μm, which is a substantial field able to induce the corresponding polarization in the ferroic layer. Since the polarization is composed of ferroelectric domains, there are two sources on inhomogeneous features in the photoinduced polarization: the bandbending, and the different orientation of polarized domains.

The sequence of events in the OCVD may occur as follows. The removal of voltage when switching off illumination depends in all cases on the disappearance of excess photogenerated carriers by recombination, that usually occurs on a time scale of 1 ms and lower. However, the change of internal vacuum level of order 1 V associated to photovoltage produces a large modification of the internal polarization structure in the device. When the electronic driving force is removed the polarization remains in an out of equilibrium state and it must decay to equilibrium configuration. For example a plausible description is that at a photovoltage close to 1 V the sample will be nearly in flatband condition in which the vacuum level is flat. By removing the photovoltage the active layer needs to develop a bandbending that will be the size of half the thickness, or even full thickness, dependending on the doping level.[15] Thus a large electrical field must be constructed with the consequent polarization. However the decay of polarization is a very slow phenomenon that will block the decrease of the voltage for a considerable time. As a reference the characteristic depolarization time τ_{dr} caused in ferroelectric oxides such as barium titanate by domain formation kinetics has typical value of 1000 s at room temperature.[20]

Regarding the slow response associated to recovery of the dark polarization, we expect that the large perturbation OCVD involves complex cooperative relaxation phenomena that give raise to non-exponential relaxation, which is a general occurrence in a broad variety of solids including polymers and glasses.[21-23] For the analysis of photovoltage decays we define here an *instantaneous relaxation time* τ_{ir} by the following expression

$$\frac{dV}{dt} = -\frac{1}{\tau_{ir}}V \tag{4}$$

Here $\tau_{ir}(V)$ describes the instantaneous advance of the relaxation, being different from the 2003 definition of Eq. (3) that applies for a recombination lifetime. In practice both curves $\tau_{ir}(V)$ and $\tau_{rec}(V)$ are rotated with respect to each other in a $\log\tau$ vs. $\log V$ plot. Implicit in Eq. (4) is that the system undergoes a decay from an initial (V_0) to final (V_1) voltage values associated to different equilibrium states of illumination intensity, namely Φ_0 and $\Phi_1 = 0$. Eq. (4) applies to the measurement of OCVD and more generally, for $\Phi_1 > 0$, at the right hand side of Eq. (4) it must be written

$$\frac{dV}{dt} = -\frac{1}{\tau_{ir}}(V - V_1) \tag{5}$$

We now analyze some characteristic relaxation functions shown in Fig. 1. For an exponential decay, τ_{ir} is a constant, consequently that the curve is horizontal. The double exponential decay in $\tau_{ir}(V)$ representation, Fig. 1(a), shows a rapid step transition from the fast to the slow time constant. There are different relaxation models in which the decay is not exponential but behaves asymptotically as a power law

$$V(t) = kt^{-\alpha} \tag{6}$$

and then we obtain

$$\tau_{ir} = \frac{k^{1/\alpha}}{\alpha}V^{-1/\alpha} \tag{7}$$

Fig. 1(b) shows an exponential decay at short times that turns into a power law decay at longer times.

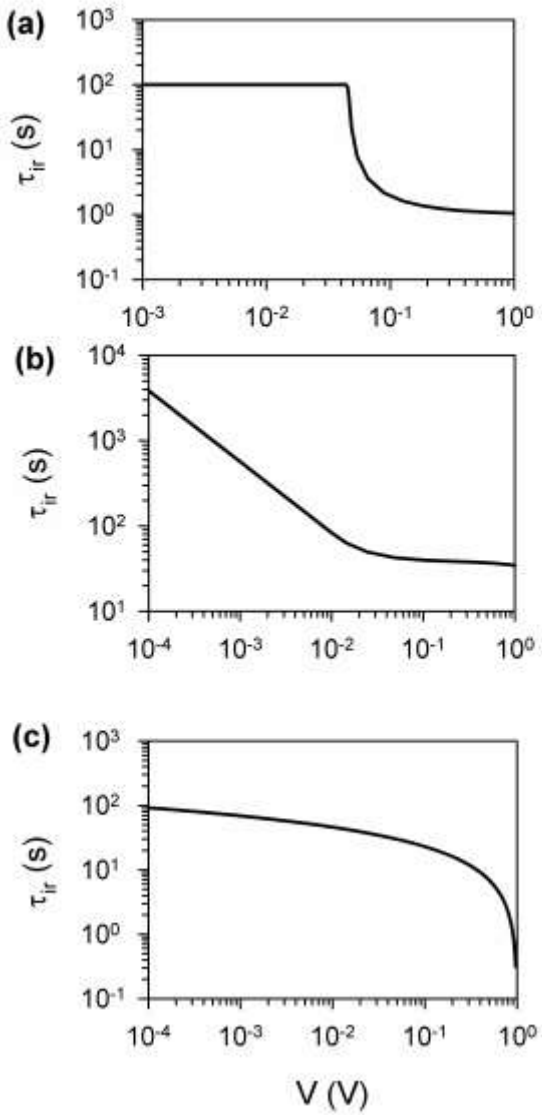

Fig. 1. Representation of instantaneous relaxation time for different types of temporal decays: (a) Double exponential decays with decay times $\tau_1 = 1$ s, $\tau_2 = 100$ s, τ_{ir} becomes constant for an exponential decay, as can be appreciated at short and long time. (b) Exponential decay at short time, $\tau = 100$ s, and power law decay with $\alpha = 1.2$ at long time. τ_{ir} becomes a straight line in log-log scale with slope -1/α. (c) Stretched exponential decay.

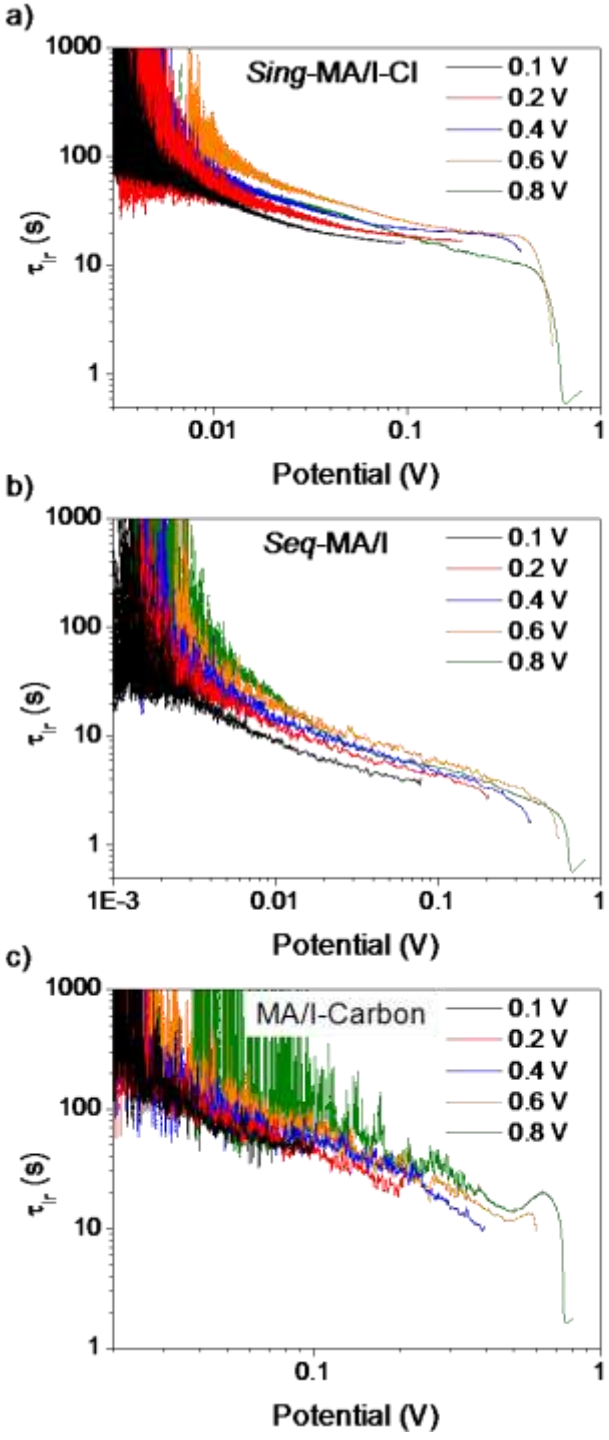

Fig. 2. Instantaneous relaxation time as function of voltage for three different $CH_3NH_3PbI_{3-x}Cl_x$ perovskite solar cells. The starting value of voltage is indicated for each cell.

The most generally used relaxation function for a cooperative solid is the Kohlrausch–Williams–Watts (KWW) stretched exponential function

$$V(t) = V_0 \exp\left[-\left(\frac{t}{\tau_0}\right)^{\beta}\right] \quad (8)$$

The instantaneous relaxation time is shown in Fig. 1(c) and it has the expression

$$\tau_{ir} = \tau_0\left[-\ln(V/V_0)\right]^{-1+1/\beta} \quad (9)$$

The representation of $\tau_{ir}(V)$ provides us the discriminative ability to separate different types of relaxation dynamics. In fact the definition of Eq. (4) is useful to assess the extent of non-exponentiality of the relaxation. We will now describe a series of OCVD results of three different types of perovskite based solar cells, fabricated as previously reported,[24-26] resulting in an average efficiency of 10%, as further described in SI. Briefly, the first set of samples analyzed consists on the single step deposition, using $PbCl_2$ precursor, of $CH_3NH_3PbI_{3-x}Cl_x$ onto a compact TiO_2/mesoporous-TiO_2 electrode and using Spiro-MeOTAD as HTM, which are denoted as *Sing*-MA/I-Cl. The second type of devices that are referred to *Seq*-MA/I were prepared by exploiting the sequential methodology, which consists on depositing by spin-coating a layer of PbI_2 onto a compact TiO_2/mesoporous-TiO_2 electrode, followed by the addition of a CH_3NH_3I solution to form the $CH_3NH_3PbI_3$ and using Spiro-MeOTAD as HTM. These two methods, configuration and materials are probably the most extended in the current literature of PSCs. The third configuration of devices consist on the deposition of $CH_3NH_3PbI_3$ by drop casting onto a meso-TiO_2/meso-ZrO_2/Carbon electrode, thus consisting on a hole conductor-free device denoted as MA/I-Carbon. This non generalized configuration is used here to validate the result in non-standard systems. The large perturbation photovoltage decays (OCVD) were registered by using a white light halogen lamp and neutral density filters to adjust the photovoltage of the cell. A mechanical shutter (≈25 ms response time) was employed for the light *On-Off* cycles and a potentiostat for the photovoltage monitoring.

The measured decays are shown in Fig. SI 1 and the correspondent instantaneous relaxation times are shown in Fig. 2. From these results we observe that perovskite solar cells with quite different morphologies display a similar pattern of the relaxation times. The first feature we observe is a rapid transition of τ_{ir} at short times (initial decay values) towards larger time scale decay. The long time decay OCVD has been reported before in perovskite solar cells in agreement with our findings.[27] In addition to the very slow decay, faster decay components occur as observed by small perturbation TPD,[26, 28] with relaxation times in the ms scale that are not detected in our OCVD experiment. Therefore, we developed complementary small perturbation transient photovoltage decays by using a white LED to vary the back illumination level and a ns-pulsed Nd/YAG laser (λ_{exc}= 650 nm) to promote the voltage perturbation (≈ 20 mV), and the results are shown in Fig. 3, while in Fig. SI 2 and 3 we show the full decay over a longer time scale. The TPD in Fig. 3 show two fast components of the decay, τ_1 and τ_2, that spans from 0.1 ms to ms. In addition, a third slower component is observed in Fig.

SI 2 and 3 which sometimes contains an overshoot of the voltage.

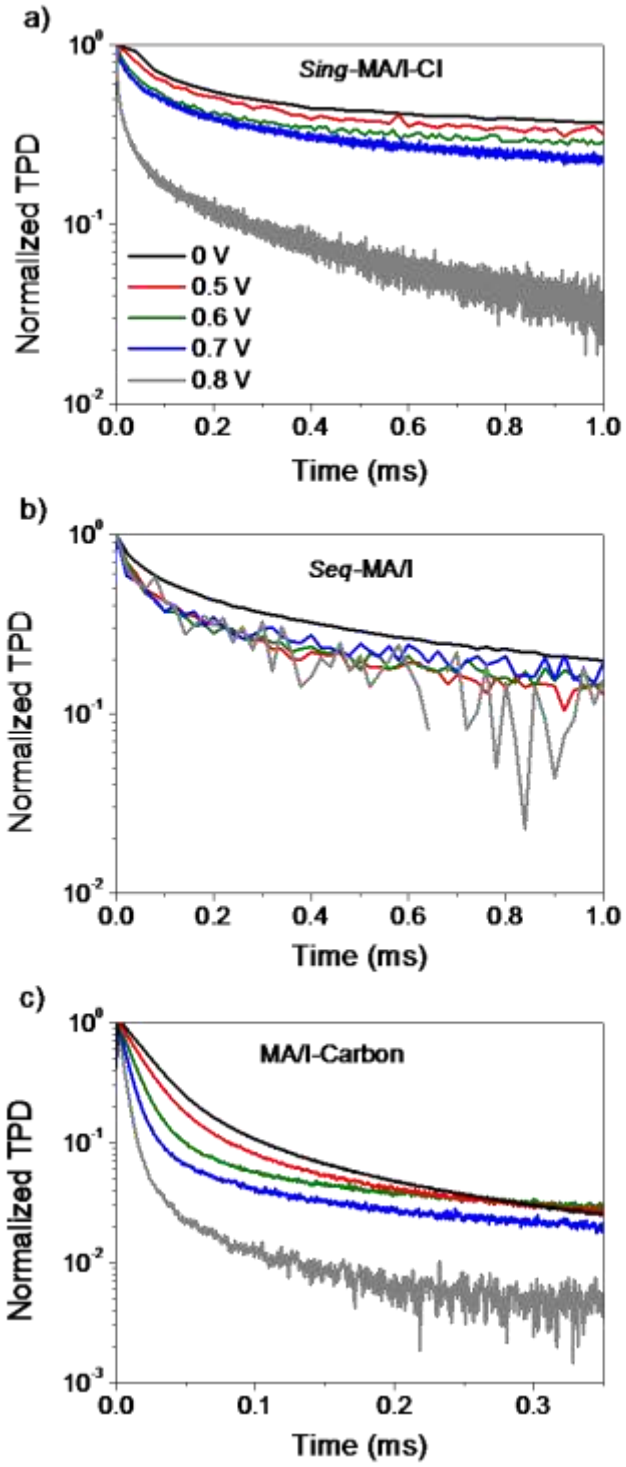

Fig. 3. Normalized small perturbation transient photovoltage decays (TPD) of three different perovskite based devices (*Sing*-MA/I-Cl, *Seq*-MA/I and MA/I-Carbon) at at voltage (from top to bottom) 0, 0.5, 0.6, 0.7, 0.8 V.

Unfortunately the resolution of TPD measurement is too low to determine the τ_{ir} using Eq. (5). However, as explained before in the expected sequence of events in a voltage decay, it makes full sense that fast decay components observed are associated to electronic phenomena, i.e., recombination-transport by charge and discharge of capacitances C_{μ} and/or C_{co}. These phenomena will be further analyzed in a forthcoming work in combination with Impedance Spectroscopy (IS) measurement, as the small perturbation IS and TPD methods should correspond to each other.

Having summarily discussed the faster components of the relaxation phenomena, we return to the analysis of the observations reported in Fig. 2. We note that the rapid increase of τ_{ir} at the highest voltage can be associated to the start of a stretched exponential relaxation. After the upward bending some cells (*Sing*-MA/I-Cl) show a nearly plateau that may show a short lived exponential relaxation that precedes a much longer feature. The most prominent feature of Fig. 2 is that in the long time all measured cells provide a power law decay, which is characteristic of a cooperative relaxation.

Remarkably, some measurements of transient behaviour in perovskite solar cells have been previously interpreted in terms of trapped electronic carriers.[19, 27, 29] The role of traps in dye-sensitized solar cells (DSC) has been widely acknowledged to cause retarded dynamics including a voltage dependence of the lifetime.[13, 30] However, in a DSC the electrons reside in a medium, meso-TiO_2, that has no holes (which lie apart in solution), and the perovskite solar cell requires different considerations. These perovskites are a type of material that contains both holes and electrons, able to directly recombine, thus we must distinguish two kinds of traps. Traps that cause long time effects need to be deep in the band gap so that the associated time of release is large. But deep traps in the middle of the gap will cause strong SRH recombination centers. It has been suggested that such traps exist in a very low number.[31] In any case one does not expect in a material containing both carriers, electrons and holes, as hybrid halide perovskite, that any kind of electronic trap can hold a significant voltage for a scale of minutes. On the other hand if the traps are shallow they remain in equilibrium with the respective band edge and they do not cause a major effect of the carrier kinetics.

In summary, we have established in this work some general patterns of depolarization kinetics of hybrid organic-inorganic perovskite solar cells. They consist on the combination of relatively fast decay phenomena of electronic origin (discharge and recombination of photogenerated electrons and holes) with a longer time decay that is related to different stable polarization states of the ferroic material at different internal voltage. We have established the presence of a power law decay relaxation time centered in the timescale 10-100 s as shown in Fig. 2. This feature may not arise from normal semiconductor traps kinetics. The shape and timescale of the decay point to a cooperative relaxation mechanism as often found in solids where molecular of structural units interact during the change of state that involves a relaxation event. The time scale is ultraslow in terms of microscopic mechanisms and we suggest that it points out to cooperative kinetics of polarization and depolarization of ferroic domains, mainly

located in depletion zones.

These findings will be an important tool for interpretation of decay features in the perovskite ferroic solar cells. There arises the important question of the interaction between the short time electronic phenomena and the global status of polarization of the sample. This issue remains for future investigation based on the present findings that establish the shape of the relaxation time of overall polarization of perovskite solar cells. This work clearly establishes the differentiate nature of perovskite solar cells in comparison with previous photovoltaic technologies. Deep understanding of the new physical phenomena occurring in these devices will be mandatory to take full advantage of the enormous potentiality of hybrid halide perovskite for the development of extremely efficient solar cells.

Supporting Information

Solar cell preparation and methods of measurement, the evolution and parameters of the experimental TPD response, the calculation and simulation of the TPD response and asymptotic behavior.

Acknowledgment

The research leading to these results has received funding from the European Union Seventh Framework Program [FP7/2007-2013] under grant agreement 316494, MINECO of Spain under project MAT2013-47192-C3-1-R) and the National Research Foundation of Korea (NRF) grants funded by the Ministry of Science, ICT & Future Planning (MSIP) of Korea under contract No. NRF-2012M3A6A7054861 (Global Frontier R&D Program on Center for Multiscale Energy System)

References

1. N. J. Jeon, J. H. Noh, Y. C. Kim, W. S. Yang, S. Ryu and S. I. Seok, *Nat Mater*, 2014, **13**, 897-903.
2. http://www.nrel.gov/ncpv/images/efficiency_chart.jpg
3. J. N. Clifford, E. Martinez-Ferrero and E. Palomares, *Journal of Materials Chemistry*, 2012, **22**, 12415-12422.
4. A. Zaban, M. Greenshtein and J. Bisquert, *ChemPhysChem*, 2003, **4**, 859-864.
5. E. J. Juarez-Perez, R. S. Sanchez, L. Badia, G. Garcia-Belmonte, Y. S. Kang, I. Mora-Sero and J. Bisquert, *J. Phys. Chem. Lett.*, 2014, ***5***, 2390-2394.
6. Y. Kutes, L. Ye, Y. Zhou, S. Pang, B. D. Huey and N. P. Padture, *The Journal of Physical Chemistry Letters*, 2014, **5**, 3335-3339.
7. R. S. Sanchez, V. Gonzalez-Pedro, J.-W. Lee, N.-G. Park, Y. S. Kang, I. Mora-Sero and J. Bisquert, *J. Phys. Chem. Lett.*, 2014, ***5***, 2357-2363.
8. R. Gottesman, E. Haltzi, L. Gouda, S. Tirosh, Y. Bouhadana, A. Zaban, E.

Mosconi and F. De Angelis, *J. Phys. Chem. Lett.*, 2014, **5**, 2662-2669.

9. J. Bisquert, D. Cahen, S. Rühle, G. Hodes and A. Zaban, *The Journal of Physical Chemistry B*, 2004, **108**, 8106-8118.

10. A. Luque, A. Marti and C. Stanley, *Nature Photonics*, 2012, **6**, 146-152.

11. J. Bisquert, A. Zaban, M. Greenshtein and I. Mora-Seró, *J. Am. Chem. Soc.*, 2004, ***126***, 13550-13559.

12. A. B. Walker, L. M. Peter, K. Lobato and P. J. Cameron, *J. Phys. Chem. B*, 2006, ***110***, 25504-25507.

13. J. Bisquert, F. Fabregat-Santiago, I. Mora-Seró, G. Garcia-Belmonte and S. Giménez, *J. Phys. Chem. C*, 2009, ***113***, 17278–17290.

14. J. Bisquert, *Physical Chemistry Chemical Physics*, 2003, **5**, 5360-5364.

15. A. Guerrero, E. J. Juarez-Perez, J. Bisquert, I. Mora-Sero and G. Garcia-Belmonte, *Applied Physics Letters*, 2014, **105**, -.

16. Y. Kawamura, H. Mashiyama and K. Hasebe, *Journal of the Physical Society of Japan*, 2002, **71**, 1694-1697.

17. A. Poglitsch and D. Weber, *The Journal of Chemical Physics*, 1987, **87**, 6373-6378.

18. J. Wei, Y. Zhao, H. Li, G. Li, J. Pan, D. Xu, Q. Zhao and D. Yu, *The Journal of Physical Chemistry Letters*, 2014, 3937-3945.

19. V. W. Bergmann, S. A. L. Weber, F. Javier Ramos, M. K. Nazeeruddin, M. Gratzel, D. Li, A. L. Domanski, I. Lieberwirth, S. Ahmad and R. Berger, *Nat Commun*, 2014, **5**.

20. M. Dawber, K. M. Rabe and J. F. Scott, *Reviews of Modern Physics*, 2005, **77**, 1083-1130.

21. C. T. Moynihan and J. Schroeder, *Journal of Non-Crystalline Solids*, 1993, **160**, 52-59.

22. V. Halpern, *Journal of Physics: Condensed Matter*, 2002, **14**, 2475.

23. C. A. Angell, K. L. Ngai, G. B. McKenna, P. F. McMillan and S. W. Martin, *Journal of Applied Physics*, 2000, **88**, 3113.

24. M. M. Lee, J. Teuscher, T. Miyasaka, T. N. Murakami and H. J. Snaith, *Science*, 2012, **338**, 643-647.

25. Y. Rong, Z. Ku, A. Mei, T. Liu, M. Xu, S. Ko, X. Li and H. Han, *The Journal of Physical Chemistry Letters*, 2014, **5**, 2160-2164.

26. J.-W. Lee, T.-Y. Lee, P. J. Yoo, M. Gratzel, S. Mhaisalkar and N.-G. Park, *Journal of Materials Chemistry A*, 2014, **2**, 9251-9259.

27. A. Baumann, K. Tvingstedt, M. C. Heiber, S. VÃ¤th, C. Momblona, H. J. Bolink and V. Dyakonov, *APL Materials*, 2014, **2**, 081501.

28. V. Roiati, S. Colella, G. Lerario, L. De Marco, A. Rizzo, A. Listorti and G. Gigli, *Energy & Environmental Science*, 2014, **7**, 1889-1894.

29. S. D. Stranks, V. M. Burlakov, T. Leijtens, J. M. Ball, A. Goriely and H. J. Snaith, *Physical Review Applied*, 2014, **2**, 034007.

30. J. Bisquert and V. S. Vikhrenko, *The Journal of Physical Chemistry B*, 2004, **108**, 2313-2322.

31. W.-J. Yin, T. Shi and Y. Yan, *Advanced Materials*, 2014, **26**, 4653-4658.

Supporting information

Cooperative kinetics of depolarization in $CH_3NH_3PbI_3$ perovskite solar cells

Luca Bertoluzzi[1], Rafael S. Sanchez[1], Linfeng Liu[2], Jin-Wook Lee[3], Elena Mas-Marza,[1] Hongwei Han[2], Nam-Gyu Park[3], Ivan Mora-Sero[1], Juan Bisquert[1,4*]

[1]Photovoltaics and Optoelectronic Devices Group, Departament de Física, Universitat Jaume I, 12071 Castelló, Spain

[2]Michael Grätzel Center for Mesoscopic Solar Cells, Wuhan National Laboratory for Optoelectronics, School of Optical and Electronic Information, Huazhong University of Science and Technology, Wuhan 430074, Hubei, People's Republic of China.

[3]School of Chemical Engineering and Department of Energy Science, Sungkyunkwan University, Suwon 440-746, South Korea

[4]Department of Chemistry, Faculty of Science, King Abdulaziz University, Jeddah, Saudi Arabia

Device fabrication

Sing-MA/I-Cl: The Fluorine-doped tin oxide substrates, FTO, (Pilkington TEC15, ≈15 Ω/sq resistance) were etched with Zn powder and HCl to obtain the desired electrode design. The substrates were thoroughly cleaned with soap (Hellmanex), deionized water and ethanol, followed by sonication in a mixture acetone: water (v/v = 1:1) and ozone cleaning. A ≈50 nm-thick TiO_2 compact layer was deposited onto FTO by aerosol spray pyrolysis at 450 ºC using a solution of titanium diisopropoxide bis(acetylacetonate) (75% in 2-propanol) diluted in ethanol (1:39, v/v) and oxygen as carrier gas. For the TiO_2 mesoporous electrodes a solution of 20-nm-sized paste (Dyesol, 90-T) diluted in terpineol (1:3, v/v) was spin-cast for 30 s at 4000 rpm and sintered at 450 ºC in air for 30 min, yielding a 200 nm-thick nanostructured film. The $MAPbI_{3-x}Cl_x$ films grown by one step methodology were prepared as reported by Snaith and co-workers.[1] In this procedure, the precursor solution was a 3:1 molar ratio mixture of MAI and $PbCl_2$ dissolved in DMF at 40%. PS films were deposited onto the mesoporous electrode by spin coating at 2000 r.p.m for 30s. The films were annealed at 100 ºC for 10 min. The deposition was carried out in the glovebox. Finally the substrates were placed in a furnace at 100 ºC under air stream, where the color of the film changed from yellow to dark brown. The hole transport solution was deposited by spin-coating of a Spiro-MeOTAD solution prepared by dissolving 72.3 mg of Spiro-MeOTAD (Merk), 28.8 µL of 4-*tert*-butylpyridine (Aldrich, 96%) and 17.5 µL of lithium bis(trifluoromethanesulfonyl)imide (LITFSI, Aldrich, 99.95%) solution (520 mg

LITSFI in 1 mL acetonitrile (Sigma-Aldrich, 99.8%)) in 1 mL of chlorobenzene (Sigma- Adrich, 99.8%). The HTM was deposited on top of perovskite substrates, by spin coating at 4000 r.p.m. for 30 s outside of the glovebox. Finally, a 60 nm-thick gold counter electrode was deposited by thermal evaporation.

Seq-MA/I: CH_3NH_3I was synthesized by reacting 0.273 mol of CH_3NH_2 with 0.223 mol of aqueous HI. The reactions were carried out in a round bottom flask for 2 h. The resulting CH_3NH_3I was collected by evaporating the solvent using a rotary evaporator at 50 ºC. The collected powder was washed with diethyl ether five times and dried in a vacuum oven for more than 12 h. FTO glasses (Pilkington, TEC-8, ≈8 Ω/sq) were cleaned by UV-ozone treatment for 15 min. The FTO substrates were further cleaned by detergent and sonication in ethanol bath for 15 min. The TiO_2 compact layer was deposited by spin-coating a solution of 0.15 M titanium diisopropoxidebis(acetylacetonate) (Aldrich, 75 wt.% in isopropanol) in 1-butanol (Aldrich, 99.8%) at 2000 r.p.m for 40 s, and dried on a hot plate at 125 ºC for 5 min. A 150 nm-thick mesoporous TiO_2 layer was formed by spin-coating the 40 nm average sized TiO_2 paste diluted with ethanol (1.4g TiO_2 paste in 10 mL ethanol) at 2000 r.p.m, and annealed at 550 ºC for 1 h. The mesoporous TiO_2 layer was further treated with 20 mM aqueous $TiCl_4$ (Aldrich, >98%) solution at 70 ºC for 10 min, which was annealed at 500 ºC for 30 min. 30 µL of 1 M PbI_2 (Aldrich, 99%) in dimethylformamide (DMF) (Sigma-Aldrich, 99.8%) solution was spin-coated on the mesoporous TiO_2 layer at 500 rpm for 5 s and 6000 rpm for 20 s, and immediately placed on hot plate at 40 ºC for 3 min and at 100 ºC for 10 min. The PbI_2 coated film was immersed in a 51.1 mM solution of CH_3NH_3I in 2-propanol (Sigma-Aldrich, 99.5%). The dipping time was 1 min. The films were spun at 500 rpm for 5s, 1500 rpm for 10s and 3000 rpm for 20 s for drying. After completion of the spin-coating cycle, the $CH_3NH_3PbI_3$ coated film was heated at 40 ºC for 3 min and 100 ºC for 10 min. To remove the excess of reagents, the films were washed with 2-propanol and dried on a hot plate for 5 min at 100 ºC. On the top of the perovskite, the hole transport layer was deposited by spin-coating a Spiro-MeOTAD solution prepared by dissolving 72.3 mg of Spiro-MeOTAD (Merk), 28.8 µL of 4-*tert*-butylpyridine (Aldrich, 96%) and 17.5 µL of lithium bis(trifluoromethanesulfonyl)imide (LITFSI, Aldrich, 99.95%) solution (520 mg LITSFI in 1 mL acetonitrile (Sigma-Aldrich, 99.8%)) in 1 mL of chlorobenzene (Sigma- Adrich, 99.8%). The Spiro-MeOTAD solution was spin-coated at 4000 r.p.m for 20 s. Finally, the gold contact was deposited by thermal evaporation at rate of 1 A/s.

MA/I-Carbon:. Mesoscopic $CH_3NH_3PbI_3/TiO_2$ solar cells were fabricated by the following process.[2, 3] FTO glass substrates (CSG Holding Co. Ltd) with high transparency in the visible range were patterned using Zn and 2M HCl aqueous solution. After cleaning the glass substrate with deionized water, ethanol and acetone using an ultrasonic bath for 15 min, successively, a compact TiO_2 layer was prepared by aerosol spray pyrolysis deposition of titanium di-isopropoxide bis(acetyl acetonate) solution in

ethanol on the glass substrate. Then a 0.8 μm porous TiO_2 layer, a 0.8 μm ZrO_2 spacer layer, and a 10 μm carbon CE were screen printed on the substrate layer by layer (the slurries were prepared following previous report).[4] The TiO_2 layer was sintered at 500 ℃ for 30 min, and the ZrO_2 and carbon layer were sintered at 400 ℃ for 30 min. The synthesis of $CH_3NH_3PbI_3$ and deposition on the monolithic device was carried out by drop-coating of a 40 wt% precursor solution onto the carbon black/graphite layer. Upon drying at 100 ℃ for 10 min, the films darkened in color, indicating the formation of $CH_3NH_3PbI_3$ in the solid state.

Device characterization.

The efficiencies were obtained through the *J/V* curves, which were recorded under AM 1.5 G (100 $mW \cdot cm^{-2}$) using a solar simulator (ABET Technologies Sun 2000) coupled with a Keithley 2400, previously calibrated with an NREL-certified Si solar cell. All the *J/V* measurements were performed by using a shadow mask of 0.1 cm^2.

Small perturbation transient photovoltage (TPD) experiments were performed by using a Nd:YAG pulsed laser (pulse duration 4-6 ns), model Brilliant (Quantel), coupled to an optical parametric oscillator (OPO), model Vibrant (Opotek), as excitation light source (650 nm). The power intensity of the laser was adjusted by using neutral density filters to afford a small perturbation of the cell photovoltage (≈ 20 mV). A white light halogen lamp and neutral density filters were employed to vary the back illumination level. The photovoltage decays were monitored by using a digital oscilloscope, model TDS5000B (Tektronix).

Results

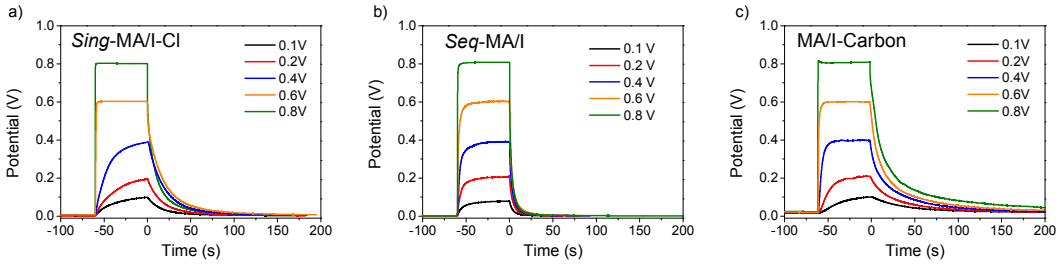

Fig. SI 1. Large perturbation V_{oc} decays at different illumination levels for the three different perovskite devices.

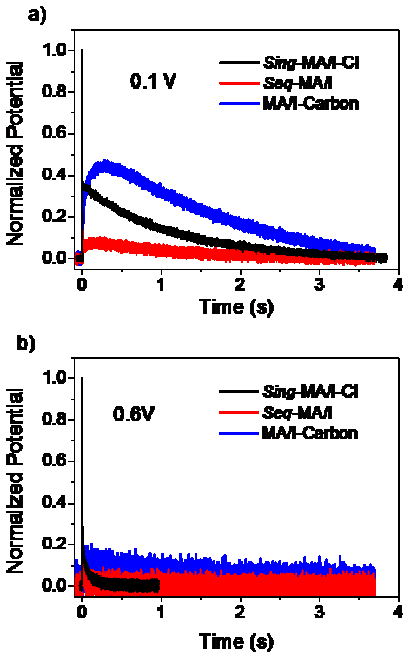

Fig. SI 2. View of second timescale of normalized small perturbation transient photovoltage decays (TPD) of three different perovskite based devices (*Sing*-MA/I-Cl, *Seq*-MA/I and MA/I-Carbon) at two different bias illumination levels; 0.1 V and 0.6 V respectively.

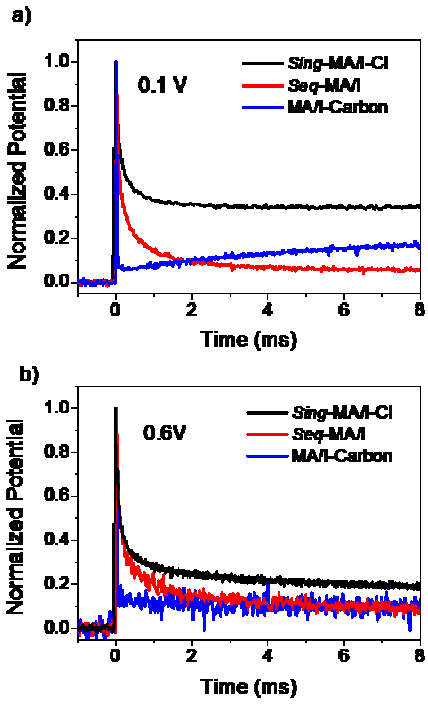

Fig. SI 3. View of ms timescale of the normalized small perturbation transient photovoltage decays (TPD) of three different perovskite based devices (*Sing*-MA/I-Cl,

Seq-MA/I and MA/I-Carbon) at two different bias illumination levels; 0.1 V and 0.6 V respectively.

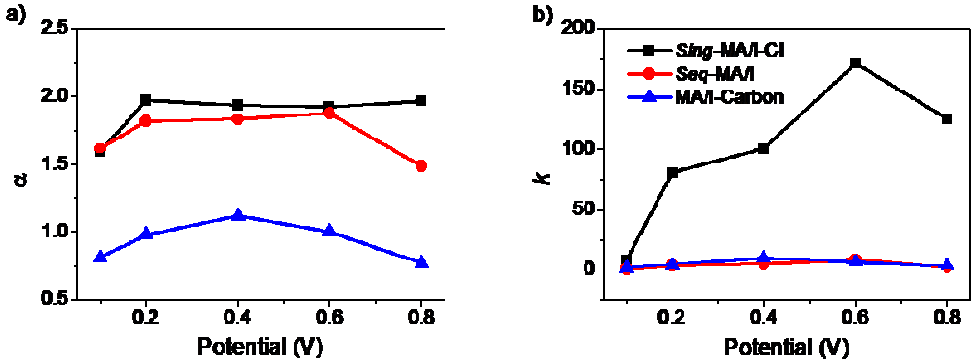

Fig. SI 4: Parameters of the power law domain in the instantaneous relaxation time τ_{ir} of Fig. 2, according to $\tau_{ir} = k^{1/\alpha} V^{-1/\alpha} / \alpha$. (a) Exponent and (b) prefactor.

References.

1. M. M. Lee, J. Teuscher, T. Miyasaka, T. N. Murakami and H. J. Snaith, *Science*, 2012, **338**, 643-647.

2. Y. Rong, Z. Ku, A. Mei, T. Liu, M. Xu, S. Ko, X. Li and H. Han, *The Journal of Physical Chemistry Letters*, 2014, **5**, 2160-2164.

3. Z. Ku, Y. Rong, M. Xu, T. Liu and H. Han, *Sci. Rep.*, 2013, ***3***.

4. A. Mei, X. Li, L. Liu, Z. Ku, T. Liu, Y. Rong, M. Xu, M. Hu, J. Chen, Y. Yang, M. Gratzel and H. Han, *Science*, 2014, **345**, 295-298.

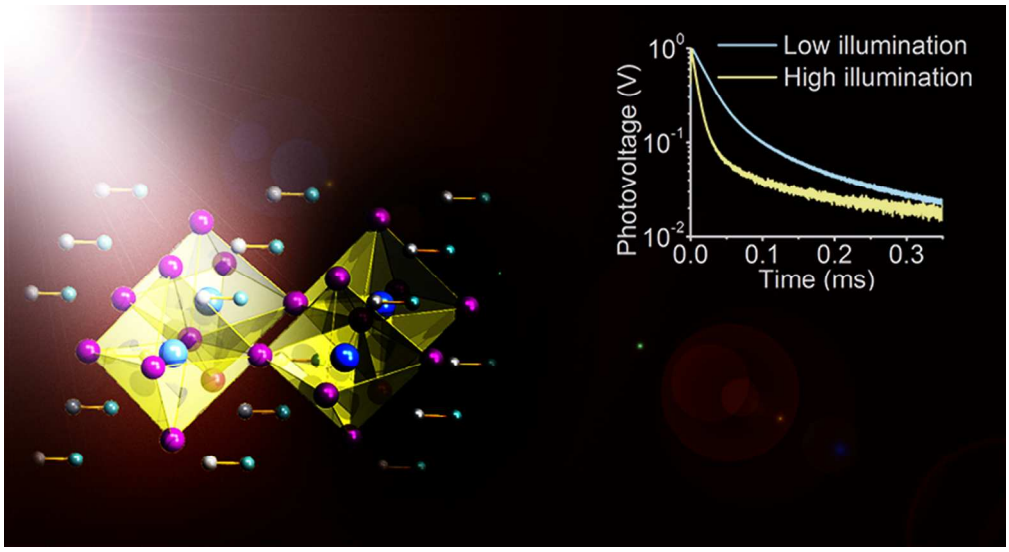

85x45mm (256 x 256 DPI)